Journal of Intelligent Material Systems and Structures

Original Article

Journal of Intelligent Material Systems and Structures
2014, Vol 25(3) 378–388

DOI: 10.1177/1045389X13498311
jim.sagepub.com
SAGE

Modeling and inverse compensation for giant magnetostrictive transducer applied in smart material electrohydrostatic actuator

Yuesong Li[1], Yuchuan Zhu[1,2], Hongtao Wu[1] and Dunbing Tang[1]

Abstract

Smart material electrohydrostatic actuator based on giant magnetostrictive transducer can meet the requirements of smaller vehicles like the unmanned combat air vehicle as well as in rotating environments like helicopter rotors. In order to analyze and improve the performance of smart material electrohydrostatic actuator, the dynamic hysteresis nonlinear model of giant magnetostrictive transducer is developed based on the relationship between complex permeability and magnetic energy power loss in giant magnetostrictive material, and the inverse model is also derived to design the inverse compensator for improving the linearity of giant magnetostrictive transducer. The experiments show that with the help of inverse compensator, phase lag between the input control signal and the output displacement of giant magnetostrictive transducer is decreased. In addition, the simulation results show that because of the effect of inverse compensator, the flow rate is increased and the growth rate increases with the increase of excitation frequency.

Keywords

Giant magnetostrictive transducer, electrohydrostatic actuator, inverse compensation, complex permeability

Introduction

Hydraulic control systems are used in aerospace and automotive industrial applications where high power density, high dynamic performance, robustness, and overload capability are desired (Karunanidhi and Sigaperumal, 2010; Li et al., 2011), but their need for hydraulic fluid lines can make them unsuitable for distributed actuation applications like those found on the unmanned combat air vehicle (UCAV) (Chaudhuri et al., 2009; Lindler and Anderson, 2003). The challenges are even greater in rotorcraft, as many of the important applications for noise and vibration control such as active flaps and active pitch links must operate in the rotating frame (John et al., 2009). A power-by-wire control system capable of large forces, large displacements, and fast responses is required in smaller vehicles like the UCAV as well as in rotating environments like helicopter rotors (Anderson and Bales, 2003). Smart material electrohydrostatic actuator (SMEHA) provides an effective way to implement this strategy (Chaudhuri and Wereley, 2012). In an SMEHA, a smart material electromechanical transducer is driven at a high frequency to pressurize fluid in a pumping chamber. The flow of the pressurized fluid is then rectified by a set of one-way valves, creating pulsing flow in a specified direction. The one-directional flow is then utilized to transfer power from the active material to a hydraulic output cylinder. The flow rectifying valves are passive valves or active valves (Lhermet et al., 2006; Sirohi and Chopra, 2003; Yoo and Wereley, 2004).

Giant magnetostrictive material (GMM) is attractive as transducer applied in SMEHA due to their high energy density, large blocked force, and wide actuation bandwidth (Chaudhuri, 2008). In addition, these actuators have no moving parts and are, therefore, mechanically less complex than conventional actuators such as hydraulic systems (Chaudhuri et al., 2009). However,

[1]Jiangsu Key Laboratory of Precision and Micro-manufacturing Technology, Nanjing University of Aeronautics and Astronautics, Nanjing, China
[2]The State Key Laboratory of Fluid Power and Mechatronic Systems, Zhejiang University, Hangzhou, China

Corresponding author:
Yuchuan Zhu, Jiangsu Key Laboratory of Precision and Micro-manufacturing Technology, Nanjing University of Aeronautics and Astronautics, Nanjing 210016, China.
Email: meeyczhu@nuaa.edu.cn

at higher actuation frequencies and magnetic fields, giant magnetostrictive transducer exhibits serious phase lag phenomenon due to hysteresis and eddy current (Armstrong, 1997; Huang et al., 2007). The phase lag makes the output displacement of giant magnetostrictive transducer lag behind the input current. If the active valves are used as flow rectifying valves whose control signals are controlled by the input current of giant magnetostrictive transducer, phase lag makes them not close and open as expected, and the oil flowing out from pump cannot all flow into cylinder. The phase lag is difficult to decrease by displacement feedback because the displacement sensor is inconveniently installed in giant magnetostrictive transducer applied in SMEHA (Li and Zhu, 2012). To improve the performance of SMEHA, it is essential to develop a dynamic nonlinear model of giant magnetostrictive transducer for using the inverse compensation to decrease the phase lag.

Based on the relationships between the complex permeability, magnetic energy stored in GMM rod, and magnetic energy losses, a dynamic nonlinear model is developed in this article. The model's parameters have definite physical meaning just like Jiles–Atherton model (Jiles, 1994), but its inverse model is much easier than inverse Jiles–Atherton model (Leite and Sadowski, 2004; Sadowski et al., 2002). The model can be used in the simulation and prediction for performance of the giant magnetostrictive transducer, and its inverse model lays a foundation for improving the performances of the giant magnetostrictive transducer and SMEHA.

Configuration of giant magnetostrictive transducer

As Figure 1 shows, SMEHA based on giant magnetostrictive transducer comprises four parts: a pump driven by giant magnetostrictive transducer, four active valves, a cylinder, and an accumulator.

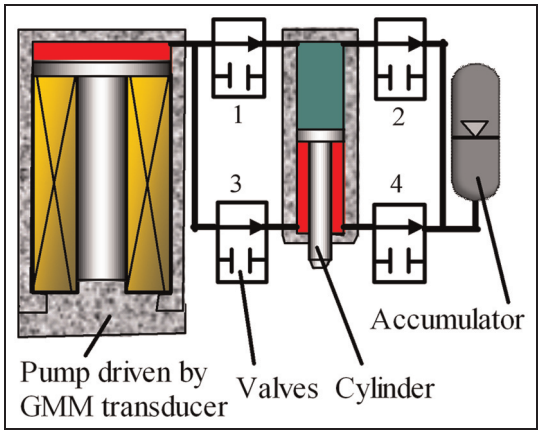

Figure 1. Schematic representation of SMEHA based on giant magnetostrictive transducer.
SMEHA: smart material electrohydrostatic actuator; GMM: giant magnetostrictive material.

The openings of active valves are controlled by a square wave to allow pressurized fluid into one of the cylinder's chambers. The square wave is controlled by the control signal of giant magnetostrictive transducer. According to the direction of cylinder's motion and the changes of pumping chamber, operation of active valves can be divided into four stages, as shown in Figure 2. The first stage is cylinder downward with compression of pumping chamber. Opening values 1 and 4, and closing values 2 and 3, the oil in pumping chamber flows into the big cavity of cylinder and the oil in the small cavity flows into accumulator. The second stage is cylinder downward with expansion of pumping chamber. Closing values 1 and 2, and opening values 3 and 4, the oil in accumulator flows into the pumping chamber. Cylinder moving upward with compression of pumping chamber is the third stage. Closing values 1 and 4, and opening values 2 and 3, the oil in pumping chamber flows into the small cavity of cylinder and the oil in the big cavity flows into accumulator. The last stage is the cylinder upward with expansion of pumping chamber. Setting values 1 and 2 open, and values 3 and 4 close, the oil in accumulator flows into pumping chamber through the big cavity of cylinder.

Figure 3 illustrates the configuration of giant magnetostrictive transducer, mainly consisting of permanent magnet, GMM rod (Terfenol-D rod is used in this research), output rod, coil, and spring. The spring applies a prestress on GMM rod because a larger magnetostrictive strain can be obtained with same magnetic field when GMM rod is compressed (Evans and Dapino, 2010). Permanent magnet is used for providing a longitudinal magnetic bias, which can improve sensitivity of GMM rod and eliminate frequency doubling. When the sign of magnetic field produced by the coil is the same as the sign of magnetic bias, the length of GMM rod elongates. If the sign of magnetic field produced by the coil and the sign of magnetic bias is opposite, GMM rod is shorter than GMM rod in initial condition.

Modeling giant magnetostrictive transducer

Dynamic magnetization model of GMM rod

In a closed magnetic circuit, the applied magnetic field H generated by an alternating current i is given by

$$H = \frac{Ni}{k_f L} = \frac{NI_m}{k_f L}\cos \omega t = H_m \cos \omega t \qquad (1)$$

The complex number form of the applied magnetic field is written as (Engdahl, 1999)

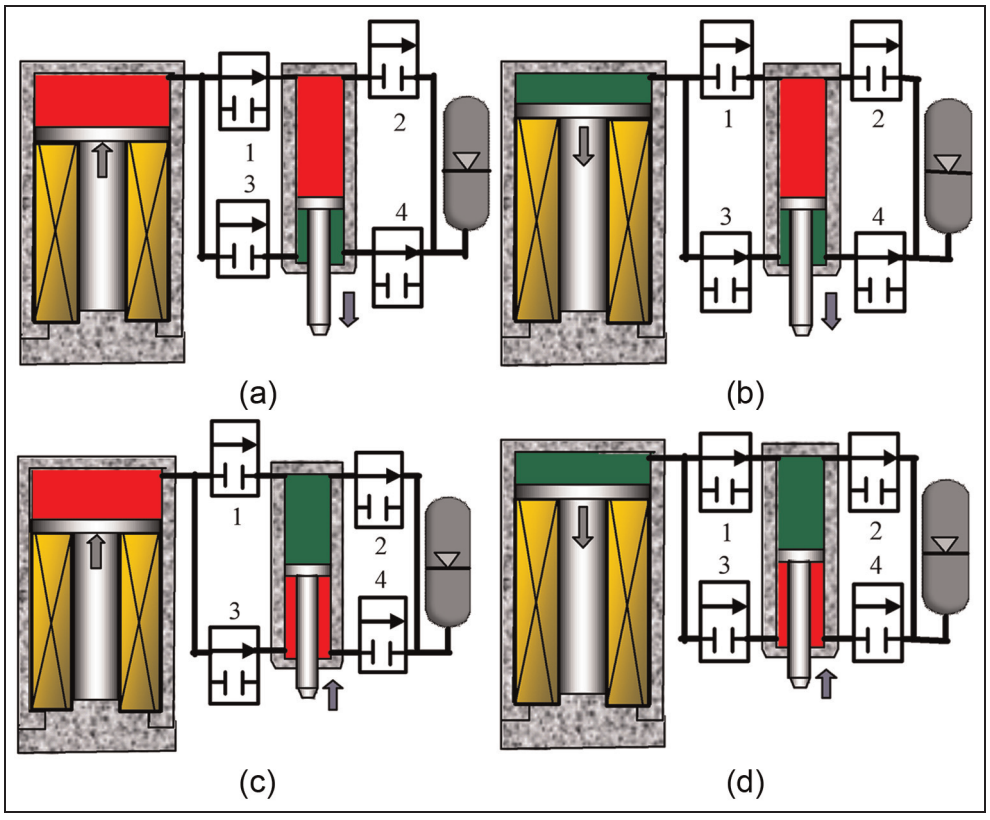

Figure 2. Operation of active valves at different stages: (a) first stage, (b) second stage, (c) third stage, and (d) fourth stage.

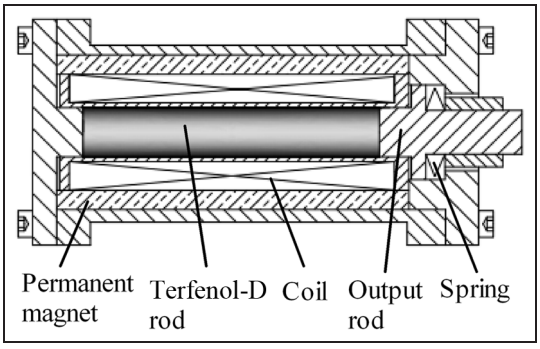

Figure 3. Configuration of giant magnetostrictive transducer.

$$\tilde{H} = H_{\mathrm{m}} e^{j\omega t} \tag{2}$$

where N is the number of the excitation coil turns, I_{m} is the amplitude of the alternating current, k_{f} is the leakage coefficient of the magnetic flux, L is the length of GMM rod, H_{m} is the amplitude of applied magnetic field, and ω is the angular frequency.

In a sinusoidal magnetic field, the relative permeability of GMM rod is a complex number, the complex number form of magnetic flux density is given by

$$\tilde{B} = \mu_0(\mu' - j\mu'')\tilde{H} = \mu_0 H_{\mathrm{m}}\left[\mu' e^{j\omega t} + \mu'' e^{j(\omega t - \pi/2)}\right] \tag{3}$$

So, the magnetic flux density B in GMM rod can be written as

$$\begin{aligned} B &= \mu_0\mu' H_{\mathrm{m}} \cos\omega t + \mu_0\mu'' H_{\mathrm{m}} \cos\left(\omega t - \frac{\pi}{2}\right) \\ &= \mu_0 H(\mu' + \mu'' \tan\omega t) \end{aligned} \tag{4}$$

where μ_0 is the permeability of free space, μ' is the real part of the complex relative permeability, μ'' is the imaginary part of the complex relative permeability.

The magnetization M can be deduced from magnetic flux density B and the applied magnetic field H

$$M = \frac{B}{\mu_0} - H = H(\mu' - 1 + \mu'' \tan\omega t) \tag{5}$$

For low magnetic fields, magnetization process of GMM rod obeys Rayleigh's law. Magnetic hysteresis power loss is given by

$$P_{\mathrm{h}} = \int_V \frac{4}{3}\mu_0\eta_0 H_{\mathrm{m}}^3 f \,\mathrm{d}V = K_{\mathrm{h}}' H_{\mathrm{m}}^3 f V \tag{6}$$

where η_0 is the Rayleigh constant, V is the volume of GMM rod, K_{h}' is the hysteresis loss coefficient at low fields, and f is the frequency of the applied magnetic field.

Due to the existence of the permanent magnet, though the applied magnetic field generated by the

alternating current may not be high, the total magnetic field is intermediate, and irreversible domain rotation takes place as the domain magnetization rotates between magnetically easy axes. Magnetic hysteresis power loss P_h is given by

$$P_h \approx \int_V K_h B_m^n f \, dV \tag{7}$$

where K_h is the hysteresis loss coefficient at intermediate fields and n is Steinmetz exponent varying from 1.5 to 2.5.

In a sinusoidal magnetic field, to reduce the classical eddy current losses, GMM rod applied in SMEHA is made in the form of laminations. The eddy current loss is calculated as follows (Jiles, 1994)

$$P_{eddy} = \int_V \frac{\gamma \delta^2}{12} \left(\frac{dB}{dt}\right)^2 dV \tag{8}$$

where γ and δ are the conductivity and the thickness of the lamination of GMM rod, respectively.

Equation (8) is derived on the conditions that magnetic flux density on the cross section of GMM rod is distributed evenly and laminations are rectangular in shape. In fact, laminations are not standard rectangles. Beyond that, the eddy current loss in the body of giant magnetostrictive transducer is not considered. Therefore, equation (8) needs to be modified by multiplying by a correction coefficient η_e as follows

$$P_{eddy} = \eta_e \int_V \frac{1}{T} \int_0^T \frac{\gamma \delta^2}{12} \left(\frac{dB}{dt}\right)^2 dt dV = K_e (B_m f)^2 V \tag{9}$$

where K_e is the eddy current loss coefficient and T is the period.

In a sinusoidal magnetic field, the excess loss which results from changes in the domain configure also need to be considered, and this component of the loss can be expressed as (Jiles, 1994)

$$P_{ex} = \int_V \sqrt{G_0 \gamma \delta w H_0} \left(\frac{dB}{dt}\right)^{1.5} dV \tag{10}$$

where w is the width of laminations, H_0 is a parameter representing the internal potential experienced by domain walls, and G_0 is a dimensionless constant of value 0.1356.

Under the restricted condition of sinusoidal variation of B with time, the excess loss can be calculated as

$$P_{ex} = \eta_{ex} \int_V \frac{1}{T} \int_0^T \sqrt{G_0 \gamma \delta w H_0} \left(\frac{dB}{dt}\right)^{1.5} dt dV = K_{ex} (B_m f)^{1.5} V \tag{11}$$

where η_{ex} is the correction coefficient and K_{ex} is the excess loss coefficient.

So, the total magnetic energy loss can be written as

$$P_{loss} = P_h + \left[K_e (B_m f)^2 + K_{ex} (B_m f)^{1.5}\right] V \tag{12}$$

Since magnetic energy loss can also be expressed as

$$P_{loss} = V \frac{1}{T} \oint H dB = \pi f \mu_0 \mu'' H_m^2 V \tag{13}$$

The imaginary part of the complex relative permeability can be calculated as follows

$$\mu'' = \frac{P_{loss}}{\pi f \mu_0 H_m^2 V} \tag{14}$$

So, at low magnetic fields

$$\mu'' = \frac{K'_h H_m^3 + K_e B_m^2 f + K_{ex} B_m^{1.5} f^{0.5}}{\pi \mu_0 H_m^2} \tag{15}$$

At intermediate magnetic fields

$$\mu'' = \frac{K_h B_m^n + K_e B_m^2 f + K_{ex} B_m^{1.5} f^{0.5}}{\pi \mu_0 H_m^2} \tag{16}$$

Equation (4) can be rewritten as follows

$$\begin{aligned} B &= \mu_0 \mu' H_m \cos \omega t + \mu_0 \mu'' H_m \sin \omega t \\ &= \mu_0 \sqrt{\mu'^2 + \mu''^2} H_m \cos(\omega t - \varphi) \end{aligned} \tag{17}$$

where φ is lag angle, and its value can be calculated as follows

$$\varphi = \arctan\left(\frac{\mu''}{\mu'}\right) \tag{18}$$

The amplitude of magnetic flux density can be obtained from equation (17)

$$B_m = \mu_0 \sqrt{\mu'^2 + \mu''^2} H_m \tag{19}$$

So, the real part of the complex relative permeability can be calculated as follows

$$\mu' = \sqrt{\left(\frac{B_m}{\mu_0 H_m}\right)^2 - \mu''^2} \tag{20}$$

Equations (16) and (20) show that B_m is the key parameter to calculate the complex permeability of GMM rod. In order to obtain the amplitude of magnetic flux density when giant magnetostrictive transducer is driven, a sensing coil is wound around the excitation coil.

The voltage of induction coil is given by

$$E = -N_c A_c \frac{dB}{dt} \tag{21}$$

where N_c is the number of sensing coil turns and A_c is the cross-sectional area of induction coil.

Due to sinusoidal variation of magnetic flux density with time, the amplitude of magnetic flux density can be obtained from equation (21)

$$B_m = \frac{E_m}{\omega N_c A_c} \tag{22}$$

where E_m is the amplitude of induced voltage.

Magnetoelastic model of GMM rod

As discussed by Li and Zhu (2012), the magnetostrictive λ is given by

$$\lambda = \frac{3}{2}\frac{\lambda_S}{M_S^2}M^2 \tag{23}$$

where λ_S and M_S are the saturation magnetostrictive and the saturation magnetization, respectively.

If an experimental point (λ_0, M_0) has been known, λ can be calculated using the following equation

$$\frac{\lambda_0}{\lambda} = \frac{M_0^2}{M^2} \tag{24}$$

Due to the existence of the permanent magnet, the complex relative permeability obtained from equation (20) and (22) is the complex relative permeability near the bias magnetic field. So, the total magnetization of GMM rod is approximately equal to the sum of bias magnetization M_b arising from the permanent magnet and magnetization M arises from the excitation coil, equation (24) can be rewritten as

$$\lambda \approx \frac{\lambda_0(M + M_b)^2}{M_0^2} = K_\lambda[H(\mu' - 1 + \mu'' \tan \omega t) + M_b]^2 \tag{25}$$

where

$$K_\lambda = \frac{\lambda_0}{M_0^2} \tag{26}$$

Kinetic model of giant magnetostrictive transducer

The lumped parameter model of giant magnetostrictive transducer is a mass–spring–damping system (Tan and Baras, 2004), as shown in Figure 4. Therefore, the model of giant magnetostrictive transducer can be described as

$$F = m\frac{d^2y}{dt^2} + c\frac{dy}{dt} + Ky \tag{27}$$

where y is the output displacement of giant magnetostrictive transducer, and m, c, and K are the equivalent mass, equivalent damping, and equivalent stiffness of giant magnetostrictive transducer, respectively.

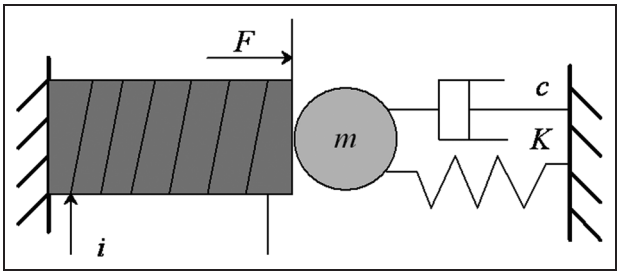

Figure 4. Lumped parameter model of giant magnetostrictive transducer.

Magnetostrictive force F is defined as

$$F = A_r E^H \lambda \tag{28}$$

where A_r and E^H are the cross-sectional area and the elastic modulus of GMM rod, respectively.

Inserting equation (28) in equation (27) and using Laplace's transforms, yields

$$y = \frac{A_r E^H \lambda}{ms^2 + cs + K} \tag{29}$$

Finally, the dynamic model of giant magnetostrictive transducer can be described as

$$y = \left[\frac{Ni}{k_f L}(\mu' - 1 + \mu'' \tan \omega t) + M_b\right]^2 \frac{A_r E^H K_\lambda}{ms^2 + cs + K} \tag{30}$$

Simulation and analysis

Simulation and experiments for giant magnetostrictive transducer

At a low excitation frequency, the output power of SMEHA is too low. But with the growth of the giant magnetostrictive transducer's excitation frequency, the output voltage and power of power amplifier are too high (Rupinsky and Dapino, 2006). So the excitation frequency for simulation and experiments is limited to 50–100 Hz in this research.

The experiment platform used for measuring the performance of giant magnetostrictive transducer is shown in Figure 5. Giant magnetostrictive transducer is driven by alternating current from power amplifier which is controlled by the sinusoidal signal generated by signal generator, and the sinusoidal signal is displayed in the oscilloscope with the output signal of displacement sensor. Due to current negative feedback, the phase of the output current of the power amplifier is synchronous with the input signal.

The voltage of induction coil is also measured by oscilloscope. Through measurement and calculation, the amplitudes of magnetic flux density under different alternating currents and frequencies are shown in

Table 1. The number of the sensing coil turns N_c is 150, the diameter of the induction coil d_c is 22 mm.

Substituting equation (20) into equation (30) and using Table 1, the output displacement becomes a function of the imaginary part of the complex relative permeability. Due to the low permeability of GMM rod (relative permeability less than 10), the imaginary part of the complex relative permeability can be obtained by varying its value from 0 to 10 to minimize the sum of the squares of the errors between the experiment values and the fitted values provided by equation (30). Substituting the obtained values into equation (16), a set of equations can be obtained, and the hysteresis loss coefficient, the eddy current loss coefficient, and the anomalous loss can be identified by solving the equations. The experiment curves used for parameter identification and the simulation curves provided by equation (30) are shown in Figure 6. In order to test the validity of the model, the experiment curves of output displacement versus input current at 50 and 100 Hz are used as test samples, and results are shown in Figure 7.

From Figures 6 and 7, some conclusions can be obtained. In the same amplitude of input current, the peak-to-peak value of output displacement decreases with the increasing of excitation frequency. Comparing with the value of 46 μm at 50 Hz, the peak-to-peak displacement of giant magnetostrictive transducer can only reach to 36 μm at 100 Hz. The experiment curves are in good agreement with simulation curves as the input current is increased from −1 to 1 A at 50–100 Hz. But when the input current decreases, the error between simulation and experiment is apparent, and it decreases with the growth of excitation frequency. The hysteresis loops of the simulation curves are symmetrical, but the hysteresis loops of experiment curves are unsymmetrical.

Analysis of power losses for giant magnetostrictive transducer

Figure 8 shows the relationship between various losses and excitation frequency. At 50–100 Hz, the excess loss P_{ex} has the lowest share of the total power loss, and its value almost does not vary with excitation frequency. The eddy current loss P_{eddy} exceeds the magnetic hysteresis loss P_h when excitation frequency is more than 50 Hz, and its value increases rapidly with the growth of excitation frequency (Table 2).

Inverse model and inverse compensation

Inverse model of giant magnetostrictive transducer

Because the input current is sinusoidal alternating, the following equation can be obtained

$$i\tan\omega t = I_m \sin\omega t = \pm\sqrt{I_m^2 - i^2} \tag{31}$$

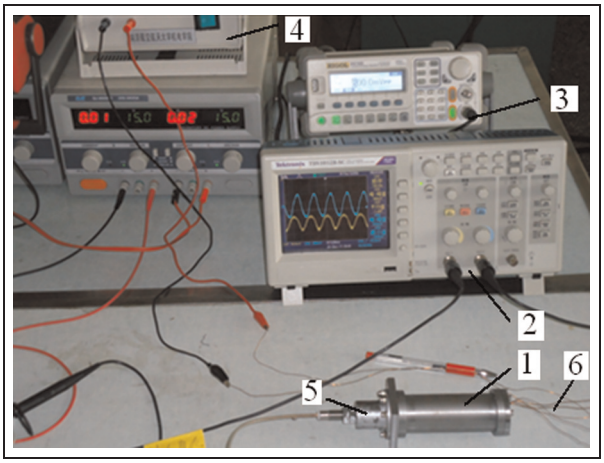

Figure 5. Photograph of the experiment platform.
1: giant magnetostrictive transducer; 2: oscilloscope; 3: signal generator; 4: power amplifier; 5: displacement sensor; 6: sensing coil.

Because the total magnetization of GMM rod is more than 0, inserting equation (31) in equation (30), the equation (30) can be rewritten as

$$i(\mu'-1)\pm\mu''\sqrt{I_m^2 - i^2} = \frac{k_f L}{N}\left(\sqrt{\frac{ms^2 + cs + K}{A_r E^H K_\lambda}}y - M_b\right) \tag{32}$$

So, if the given displacement is y_d, the input current can be calculated as the following quadratic equation

$$\left[(\mu'-1)^2 + \mu''\right]i^2 - 2(\mu'-1)\varphi_0 i + \varphi_0^2 - (I_m\mu'')^2 = 0 \tag{33}$$

where

$$\varphi_0 = \frac{k_f L}{N}\left(\sqrt{\frac{m\frac{d^2y_d}{dt^2} + c\frac{dy_d}{dt} + Ky_d}{A_r E^H K_\lambda}} - M_b\right) \tag{34}$$

The roots of equation (33) are

$$i = \frac{\varphi_0(\mu'-1) - \varphi_1}{(\mu'-1)^2 + (\mu'')^2} \tag{35}$$

$$i = \frac{\varphi_0(\mu'-1) + \varphi_1}{(\mu'-1)^2 + (\mu'')^2} \tag{36}$$

where

$$\varphi_1 = \sqrt{\varphi_0^2(\mu'-1)^2 - \left[(\mu'-1)^2 + (\mu'')^2\right]\left[\varphi_0^2 - (I_m\mu'')^2\right]} \tag{37}$$

If the given displacement is increasing, the input current are calculated by equation (35), else the input current are calculated by equation (36).

Table 1. Amplitudes of magnetic flux density by measuring and calculating.

f (Hz)	I_m (A)	E_m (V)	B_m (T)
5	0.5	0.053	0.0300
5	0.7	0.095	0.0530
50	1.0	1.140	0.0637
70	1.0	1.500	0.0590
80	1.0	1.620	0.0570
100	1.0	1.900	0.0531

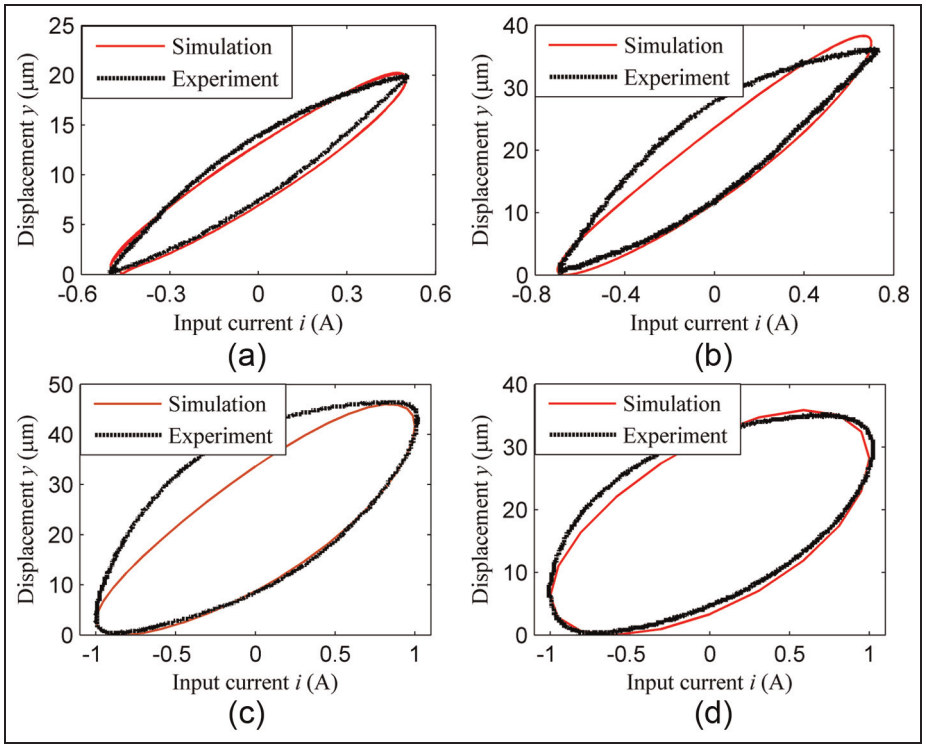

Figure 6. Output displacement versus input current used for parameter identification: (a) 5, (b) 5, (c) 50, and (d) 100 Hz.

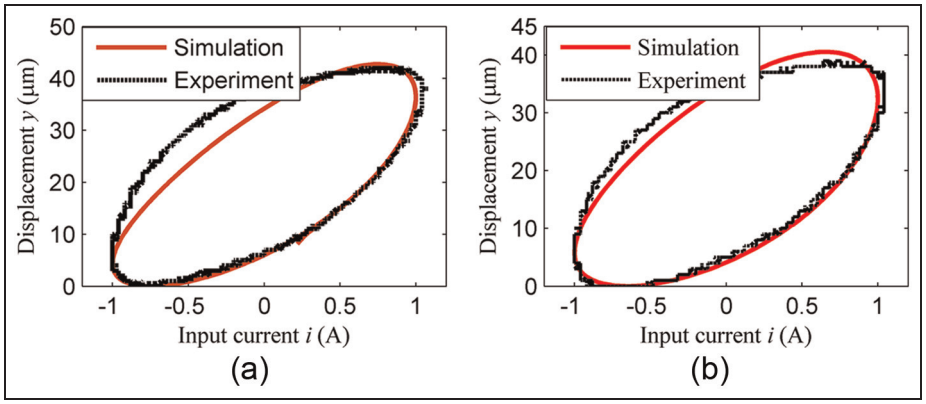

Figure 7. Output displacement versus input current used for model checking: (a) 70 and (b) 80 Hz.

Table 2. Simulation parameters for giant magnetostrictive transducer.

Parameters	Value
Diameter of GMM rod (d) (mm)	10
Length of GMM rod (L) (mm)	80
Equivalent mass of giant magnetostrictive transducer (m) (kg)	0.02
Equivalent damping of giant magnetostrictive transducer (c) (N s/m)	2945
Equivalent stiffness of giant magnetostrictive transducer (K) (N/m)	1.963×10^7
Bias magnetization (M_b) (kA/m)	250
Number of the excitation coil (N) (turns)	1300
Hysteresis loss coefficient (K_h)	85805
Steinmetz exponent (n)	1.8092
Eddy current loss coefficient (K_e)	2753.39
Anomalous loss coefficient (K_{ex})	895.80
Constant (K_λ) (m^2/A^2)	1.4694×10^{-14}
Number of the sensing coil (N_c) (turns)	150
Cross-sectional area of the sensing coil (A_c) (mm^2)	380
Leakage coefficient of the magnetic flux (K_f)	1.1
Cross-sectional area of the pump's piston (A_d) (mm^2)	1256

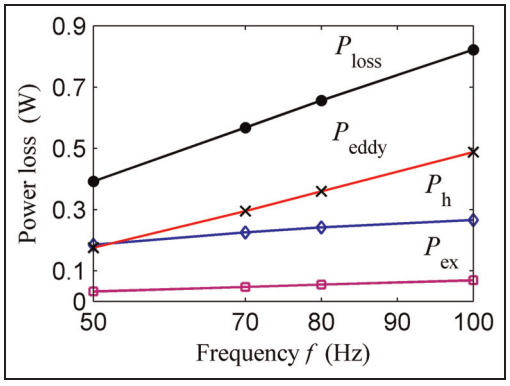

Figure 8. The power losses versus excitation frequency.

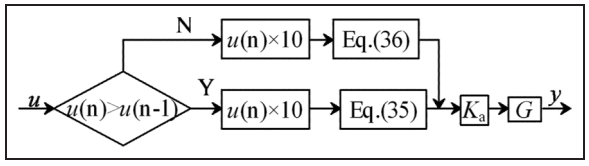

Figure 9. Flowchart of inverse compensation control for giant magnetostrictive transducer.

Inverse compensation for giant magnetostrictive transducer

Figure 9 illustrates the flowchart of inverse compensator for giant magnetostrictive transducer. Ten times the input signal u is the given displacement y_d. $u(n)$ and $u(n-1)$ are the sampling values, if $u(n) > u(n-1)$, the input current is calculated by equation (35), else the control current is obtained from equation (36). G is the plant of giant magnetostrictive transducer, and K_a is the gain of power amplifier, $K_a = 1$.

Letting input control signal $u = 2.2 + 2.2\cos 100\pi t$, $u = 1.9 + 1.9\cos 140\pi t$, $u = 1.7 + 1.7\cos 160\pi t$, $u = 1.5 + 1.5\cos 200\pi t$, respectively, the relationship between the output displacement of giant magnetostrictive transducer with inverse compensator and input control signal u can be obtained by experiments. The experiment curves are shown in Figure 10.

In order to analyze the performance of the inverse compensation method, it is necessary to get the contrast curves of the uncompensated and compensated displacements under different frequencies. However, the control signal of uncompensated displacement equals to input current, and 10 times the control signal of compensated displacement equals to the given displacement. So, before plotting the contrast curves in the same figures, the experimental data need normalizing. The data normalization method is given by

$$X_i = \frac{x_i - x_{\min}}{x_{\max} - x_{\min}} \tag{38}$$

where x_i are the experimental data, $x_{\min}$ is the minimum in experimental data, $x_{\max}$ is the maximum in experimental data, and X_i are the normalized data.

With the help of inverse compensator, the linearity between input control signal u and the output displacement y is improved significantly, as shown in Figures 10 and 11. However, the displacement does not decrease in the proportion to the control signal at 50, 70, and 80 Hz. The reason is that the model at decreasing regions is imprecise. Because the requirement for control signal is that the displacement of giant magnetostrictive transducer takes its minimum value when the control signal gets trough, and the displacement gets the maximum value when the control signal is at its peaks. So, the inverse compensating method shown in Figure 9 can be used in the inverse compensation for giant magnetostrictive transducer on SMEHA.

Effect of inverse compensation on SMEHA

The flow rate q which flows into cylinder is given by (Chaudhuri, 2008; Yoo et al., 2005)

$$q = fA_d\Delta y \tag{39}$$

where A_d is the cross-sectional area of the pump's piston, Δy is the incremental displacements of giant magnetostrictive transducer with the control signal varying from the minimum to maximum.

Regardless of time delay of active valves, pump is driven by giant magnetostrictive transducer without inverse compensator, the control signal of square wave controlling valves is the same signal which controls the excitation current, and the flow rate flowing into cylinder is given by

$$q = fA_d\left(y|_{i=1} - y|_{i=-1}\right) \tag{40}$$

However, when the pump is driven by giant magnetostrictive transducer with inverse compensator, the control signal of square wave controlling valves is the signal which has a better linearity with the output displacement, the flow rate flowing into cylinder can be written as

$$q' = fA_d\left(y|_{u=u_m} - y|_{u=0}\right) \tag{41}$$

The displacements in equations (40) and (41) can be obtained from Figures 6, 7, and 10. The values under different frequencies are shown in Table 3.

Substituting the output displacement in Table 3 into equations (40) and (41), the flow rate corresponding to the uncompensated and the compensated giant magnetostrictive transducers can be calculated. The calculation of the flow rates under different frequencies are plotted in Figure 12.

Figure 12 shows that the flow rate is improved with the help of inverse compensator and the growth rate of the flow rate increases with excitation frequency. The reason is that the phase lag between the input current and the displacement at a higher excitation frequency is more serious.

Conclusion

1. On the condition that the applied magnetic field is sinusoidal alternating, the relative permeability of GMM rod is a complex number, its imaginary part can be obtained from magnetic energy power loss, and its real part can be derived from the relationship between the amplitude of magnetic flux density and relative permeability. The amplitude of magnetic flux

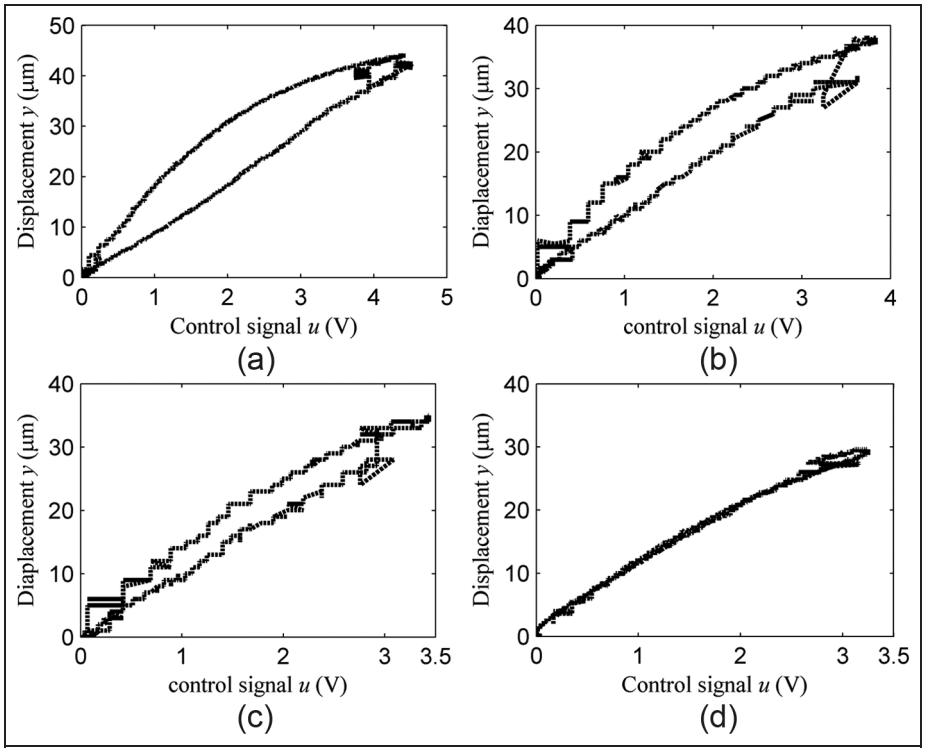

Figure 10. Curves of the compensated displacements versus input control signal u under different frequencies: (a) 50, (b) 70, (c) 80, and (d) 100 Hz.

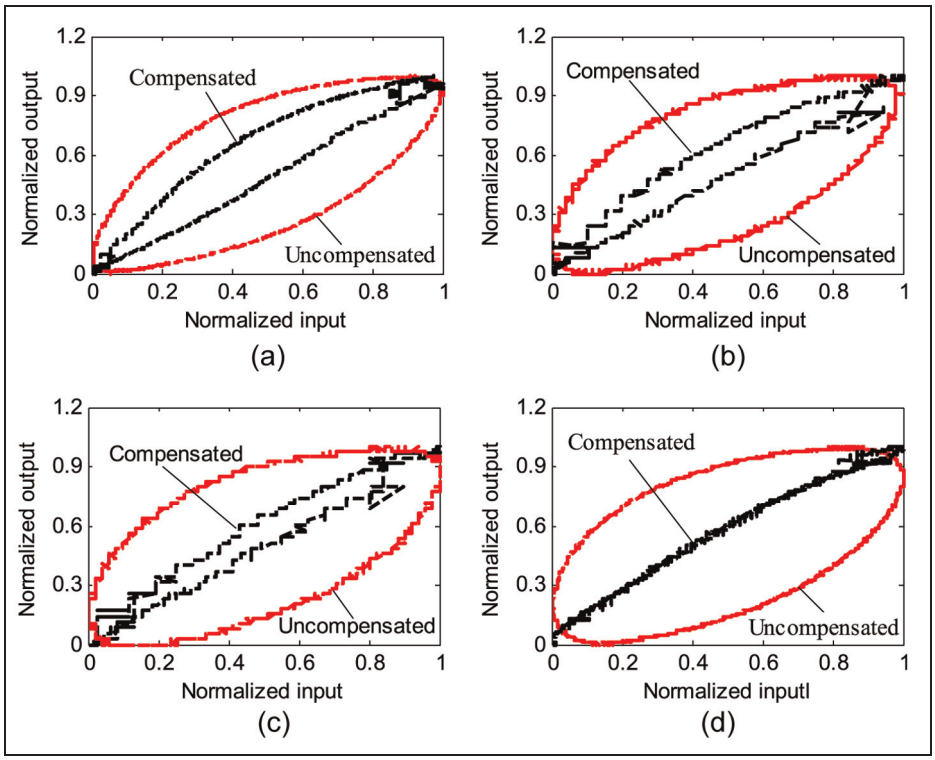

Figure 11. Contrast curves of the uncompensated and compensated displacements under different frequencies: (a) 50, (b) 70, (c) 80, and (d) 100 Hz.

Table 3. Displacements under different maximum and minimum control signals.

f (Hz)	$y\|_{i=1}$ (μm)	$y\|_{i=-1}$ (μm)	$y\|_{u=0}$ (μm)	$y\|_{u=u_m}$ (μm)
50	42	1.8	0	46
70	38	3	0	42
80	36	4	0	40
100	31.2	4.6	0	35.2

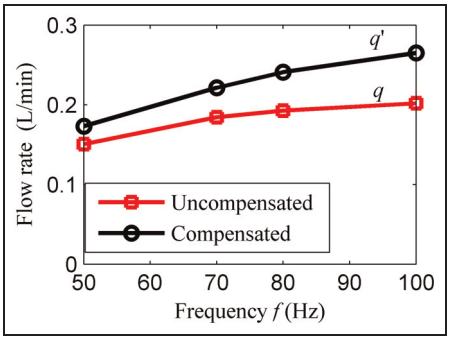

Figure 12. Flow rate versus frequencies under the uncompensated and compensated displacements.

density is proportion to the amplitude of induced voltage of a sensing coil winded around the excitation coil.

2. The experiment curves agree with simulation curves as the input current is increased from −1 to 1 A at 50–100 Hz, but when the input current is decreased, the error between simulation and experiment is apparent at 50–80 Hz. As the excitation frequency increases, the power loss and the imaginary part of permeability increase and the amplitude of output displacement decreases. The eddy current loss exceeds magnetic hysteresis loss and accounts for the biggest proportion of the total power loss at a higher frequency than 50 Hz. Comparing with the hysteresis loop of the simulation curves, the hysteresis loop of the experiment curves is unsymmetrical.
3. The compensator based on inverse model can improve the linearity between input control signal and the output displacement significantly. The accuracy of model has a large effect on the performance of inverse compensator, so unlike at 100 Hz, the displacement does not decrease in the proportion to the control signal at 50 Hz.
4. With the help of inverse compensator, the flow rate is improved and the growth rate of the flow rate increases with the increase of excitation frequency. So, the performance of SMEHA can be

improved by inverse compensation for giant magnetostrictive transducer.

Funding

This work was supported by the National Natural Science Foundation of China (grant number 51175243); the Aeronautical Science Foundation of China (grant number 20110752006); the Visiting Scholar Foundation of Key Lab in University of China (grant number GZKF-201116); the Funding of Jiangsu Innovation Program for Graduate Education (grant number CXZZ11_0196) the Funding of Jiangsu for Distinguished Young Scholar (grant number BK201210111); and the NUAA Fundamental Research Funds (grant number NS2013046).

References

Anderson EH and Bales GL (2003) Application of smart material-hydraulic actuators. *Proceedings of SPIE* 5054: 73–84.

Armstrong WD (1997) Magnetization and magnetostriction processes in Tb(0.27-0.30)Dy(0.73-0.70)Fe(1.9-2.0). *Journal of Applied Physics* 81: 2321–2331.

Chaudhuri A (2008) *Self-contained hybrid electro-hydraulic actuators using magnetostrictive and electrostrictive materials*. PhD Thesis, University of Maryland, College Park, MD.

Chaudhuri A and Wereley NM (2012) Compact hybrid electro-hydraulic actuators using smart materials: a review. *Journal of Intelligent Material Systems and Structures* 23: 597–634.

Chaudhuri A, Yoo JH and Wereley NM (2009) Design, test and model of a hybrid magnetostrictive hydraulic actuator. *Smart Materials and Structures* 18: 964–1726.

Engdahl G (1999) *Handbook of Giant Magnetostrictive Materials*. San Diego, CA: Academic Press.

Evans PG and Dapino MJ (2010) Efficient magnetic hysteresis model for field and stress application in magnetostrictive Galfenol. *Journal of Applied Physics* 107: 3906–3917.

Huang WM, Wang BW and Cao SY (2007) Dynamic strain model with eddy current effects for giant magnetostrictive transducer. *IEEE Transactions on Magnetics* 43: 1381–1384.

Jiles DC (1994) Modelling the effects of eddy current losses on frequency dependent hysteresis in electrically conducting media. *IEEE Transactions on Magnetics* 30: 4326–4328.

John S, Chaudhuri A, Cadou C, et al. (2009) Unsteady fluid flow in hybrid hydraulic actuator. *Journal of Intelligent Material Systems and Structures* 20: 2201–2214.

Karunanidhi S and Sigaperumal M (2010) Design, analysis and simulation of magnetostrictive actuator and its application to high dynamic servo valve. *Sensors and Actuators A: Physical* 157: 185–197.

Leite JV and Sadowski N (2004) Inverse Jiles-Atherton vector hysteresis model. *IEEE Transactions on Magnetics* 40: 1769–1775.

Lhermet N, Delas O and Claeyssen F (2006) Magnetostrictive pump with piezo active valves for more electrical aircraft. In: *10th international conference on new actuators*, June 2006, Bremen, Germany, vol. 144, pp. 964–967.

Li YS and Zhu YC (2012) Research on displacement-sensing model and hysteresis loop of giant magnetostrictive actuator. *Journal of Mechanical Engineering* 48: 169–174.

Li YS, Zhu YC and Wu HT (2011) Parameter optimization of jet-pipe servovalve driven by giant magnetostrictive actuator. *Acta Aeronautica et Astronautica Sinica* 32: 1336–1344.

Lindler JE and Anderson EH (2003) Design and testing of piezoelectric-hydraulic actuators. *Proceedings of SPIE* 5054: 53–65.

Rupinsky MJ and Dapino MJ (2006) Smart material electrohydrostatic actuator for intelligent transportation systems. In: *Proceedings of ASME IMECE*, vol. 145, Paper no. 14542, 5–10 November, Chicago, IL pp. 421–431.

Sadowski N, Batistela NJ, Bastos JP, et al. (2002) An inverse Jiles-Atherton model to take into account hysteresis in time-stepping finite-element calculations. *IEEE Transactions on Magnetics* 38: 797–800.

Sirohi J and Chopra I (2003) Design and development of a high pimping frequency piezoelectric-hydraulic hybrid actuator. *Journal of Intelligent Material Systems and Structures* 14: 135–147.

Tan X and Baras JS (2004) Modeling and control of hysteresis in magnetostrictive actuators. *Automatica* 40: 1469–1480.

Yoo JH and Wereley NM (2004) Performance of a magnetorheological hydraulic power actuation system. *Journal of Intelligent Material Systems and Structures* 15: 847–858.

Yoo JH, Sirohi J and Wereley NM (2005) A magnetorheological piezohydraulic actuator. *Journal of Intelligent Material Systems and Structures* 16: 945–953.